applied sciences

MDPI

Article

Research on the Recognition Method of Dial Scales for Arrester Pointer Instruments Based on Deep Learning

Huaiwen Wang [1], Yang Hu [1], Honghuan Yin [1,*] and Yue Cui [2,*]

[1] Tianjin Key Laboratory of Refrigeration Technology, Tianjin University of Commerce, No. 409 Guangrong Road, Beichen District, Tianjin 300134, China; wanghw@tjcu.edu.cn (H.W.); huyang@stu.tjcu.edu.cn (Y.H.)
[2] Department of State-Owned Assets and Laboratory Management, Tianjin University of Commerce, No. 409 Guangrong Road, Beichen District, Tianjin 300134, China
* Correspondence: yinhonghuan@tjcu.edu.cn (H.Y.); cuiyue@tjcu.edu.cn (Y.C.)

Abstract: To address the recognition challenges faced by arrester pointer instruments' dial scales in various scenarios, this paper introduces a deep learning-based recognition method for pointer instrument scales. An attention module is integrated into the YOLOv5 network architecture, enhancing the accuracy and robustness of the model. After correcting the dial, dial recognition is conducted with OpenCV to achieve precise identification of the instrument scales. The proposed method was tested using images of arrester pointer instruments against diverse backgrounds. The experimental results demonstrate that the method processes instrument data images in an average time of 0.662 s and achieves a successful recognition rate of 96% with an average error of 0.923%. This method provides a rapid and efficient approach for recognizing instrument scales and offers a novel solution for identifying similar types of instruments.

Keywords: deep learning; pointer instrument; YOLOv5; attention mechanism; OpenCV

check for updates

Citation: Wang, H.; Hu, Y.; Yin, H.; Cui, Y. Research on the Recognition Method of Dial Scales for Arrester Pointer Instruments Based on Deep Learning. *Appl. Sci.* **2024**, *14*, 2049. https://doi.org/10.3390/app14052049

Academic Editor: Jin-Yeon Kim

Received: 2 February 2024
Revised: 21 February 2024
Accepted: 27 February 2024
Published: 29 February 2024

1. Introduction

To ensure the optimal functioning of substation facilities, real-time monitoring of the operational status of arresters is crucial. Owing to their consistent data display, straightforward structure, and superior anti-interference capabilities, pointer instruments are extensively utilized in substations. However, traditionally, the reading of instrument scales typically necessitates manual operations at predetermined intervals, a method that is not only labor-intensive but also susceptible to omissions and errors. With advancements in technology, intelligent scale recognition systems for instruments are increasingly supplanting manual operations, demonstrating the capability to efficiently and accurately carry out the tasks of reading and recording scales in substations.

Currently, in the research of scale recognition for instruments, researchers have proposed solutions from different perspectives. Huo et al., have developed an innovative method that employs computer vision techniques for the detection of pointers and the recognition of indicator numbers. In this method, the characteristic features of the instrument's pointer are extracted from an image that has undergone preliminary processing. This is performed by applying the rules of Freeman chain code encoding. The indicator number associated with the pointer is determined by analyzing its angular position [1]. Li et al., have introduced an optimized three-point-based circle determination method for calibrating the dial center and segmenting the dial, and they also propose an improved angle method to facilitate the automatic reading recognition of pointer instruments [2]. Wang has created an automated system for recognizing pointer meters that capitalizes on line scan vision technology. This system employs the light-spot centroid algorithm to accurately determine the central point of the meter's pointer. Trials have demonstrated that this method for extracting data from pointer meters exhibits remarkable resilience against various disturbances [3]. Ma et al., have introduced a highly precise and sturdy algorithm for the automatic reading of pointer meters. Their innovative approach involves a new method for setting the binarization threshold, which is based on symmetry levels to segment the region of the pointer, successfully overcoming issues related to the shadow of the pointer [4]. Peng et al., have introduced a method for recognizing pointer instruments that uses Fourier transform to speed up convolution processes and improve cosine similarity measures. By utilizing statistics of grid motion, this technique efficiently removes incorrect match points and assists in the refined alignment of the image, thereby greatly improving the speed of identification for pointer instruments [5]. Li et al., have developed an algorithm for reading dial gauges based on coordinate positioning, which tackles the challenges posed by irregular lighting, intricate dial backgrounds, and the interference from damping fluids in the gathered images of the instruments. The results of their experiments confirm that this algorithm successfully identifies the circle's center and the gauge pointer, enabling the automatic acquisition of readings [6]. Guo et al., have presented a smart approach for reading indications on pointer meters and automating data gathering, utilizing machine vision combined with wireless sensor network (WSN) technology. Findings indicate that their method for detecting pointers shows enhanced robustness and superior resistance to interference when compared to traditional image segmentation and skeletonization techniques [7]. Yang et al., have proposed a real-time system for reading single-point analog meters, employing the YolactEdge instance segmentation framework, which has been executed and operationalized on the Jetson Xavier NX edge computing device [8].

The traditional recognition techniques previously mentioned are heavily reliant on the use of either isolated or manually configured features to accurately pinpoint the scales present on various instruments. However, these methods tend to fall short when subjected to environments characterized by their complexity and a high degree of variability, where their performance in terms of accuracy and robustness is often compromised. In the realm of pointer detection, a favored approach is the application of the Hough transform algorithm. Despite its widespread use, this algorithm is notably susceptible to the detrimental effects of image noise, resulting in a performance that is less than ideal in terms of its anti-interference properties.

With the advancement of deep learning, numerous detection algorithms stemming from this field have been proposed, including the YOLO series [9–13] and the R-CNN series [14–18]. Wu et al., have developed the YOLOX-CAlite algorithm for meter detection to address the specific performance challenges encountered in target detection within the context of meter reading. The tests conducted demonstrated that this refined YOLOX-CAlite version reached an average precision (AP) rate of 90.4% [9]. Zhang et al., have suggested a technique that combines Yolov7 with the Hough transform for the recognition of pointer meters, aiming to improve their automatic readability. The model's mean Average Precision (mAP) on the instrument dataset using Yolov7 has achieved an impressive high of 99.8%. Moreover, the accuracy of the readings from pointers using this technique surpasses 95%, indicating its potential for extensive application in numerous situations [10]. Liu et al., have engineered a smart recognition technology for pointer instruments that leverages YOLOv5, enabling swift location and reading identification of these instruments [11]. Chen et al., have presented a smart vision recognition approach that integrates YOLOv5 with the U-2-Net network (YLU2-Net) to boost the precision and speed of meter identification in intricate settings. The trials conducted validate the effectiveness and performance of the YLU2-Net method they propose [12]. Zhang et al., have developed a technique that utilizes YOLOv3 for the categorization and reading detection of industrial instruments, capable of interpreting both pointer-type and digital meters [13]. Liu et al., have introduced a flexible detection and identification system for pointer meters using computer vision, adaptable to a range of settings. The system employs a Faster Region-based Convolutional Network (Faster R-CNN) to accurately identify the location of the meter of interest, subsequently adjusting the camera according to the detection box. Test outcomes show the system's reliability and precision, verifying its effectiveness across diverse scenarios [14]. Cai et al., have put forward a recognition model that utilizes convolutional neural networks along with a unique virtual sample creation technology. This technology can produce a multitude of images from a small number of actual instrument images, effectively facilitating the training of the recognition model [15]. Zuo et al., have presented a novel and reliable method for recognizing readings on pointer meters, achieving autonomous recognition [16]. Hou et al., have introduced an innovative method for recognizing pointer meters that combines lightweight convolutional neural networks (CNN) with wireless sensor networks (WSNs). This approach encompasses image pre-processing, CNN-based classification, and calculation of readings at the WSN endpoint, which notably decreases data transmission by sending only the recognized outcome across the WSN [17]. Wang et al., have explored an automatic method for reading industrial pointer meters to tackle present challenges, by incorporating object detection through the Faster Region-based Convolutional Network (Faster-RCNN) combined with classic computer vision techniques [18]. Zhou et al., have put forward an innovative intelligent end-to-end method for reading pointer meters utilizing deep learning techniques. This approach identifies the meter and captures the pointer concurrently without the need for pre-existing information. Tests demonstrate that this method outperforms several standard methods in both speed and efficacy [19]. Wang et al., have developed a Lite-FCOS guided by scale value for recognizing readings from pointer meters, employing Hough transform and analysis of pointer distribution to ascertain the direction of the meter pointer [20].

Within the realm of these algorithms, R-CNN stands as a foundational approach to region-based object detection, a process which partitions the task of detection into discrete phases: initially, the algorithm identifies areas within an image that potentially contain objects—a step known as target localization. Subsequently, it classifies each localized region into specific categories depending on the objects they are believed to contain. The R-CNN and its subsequent iterations, such as Fast R-CNN and Faster R-CNN, leverage this two-stage strategy to fine-tune the precision of object detection. They are particularly adept at discerning intricate details and managing the presence of small or overlapping objects against complex backgrounds. However, the increased accuracy offered by these algorithms comes at the price of computational efficiency; the need to generate and individually analyze multiple region proposals for each image makes them less suitable for applications requiring swift decision-making in real-time scenarios. YOLO (You Only Look Once) exemplifies the single-stage object detection paradigm, eschewing the multi-stage process in favor of a unified, holistic approach. YOLO transforms the task of object detection into a solitary regression challenge, concurrently determining the bounding boxes and class probabilities in one go directly from entire images. This streamlined method significantly accelerates the detection process, offering a considerable advantage in scenarios where real-time processing is crucial.

To minimize environmental interference on measurement accuracy and boost the precision and robustness of arrester instrument scale recognition, this study introduces a deep learning-based recognition method. The schematic diagram of the research methodology for this study is shown in Figure 1.

In this paper, the Methods section delves into the technical aspects of the proposed solution, detailing the integration of attention mechanisms into the YOLOv5 model and the subsequent steps for instrument scale recognition. In the Results section, the outcomes of the experimental evaluation of the proposed method on a specialized dataset will be presented. Metrics such as precision, recall, and mean average precision are used to quantify the model's performance. The Discussion section interprets the significance of the study's findings, noting the high success rate in recognition and the positive impact of attention mechanisms on model accuracy. The Conclusion section encapsulates the main achievements of the research, emphasizing the practical implications for substation monitoring automation and suggesting avenues for future development in intelligent industrial systems.

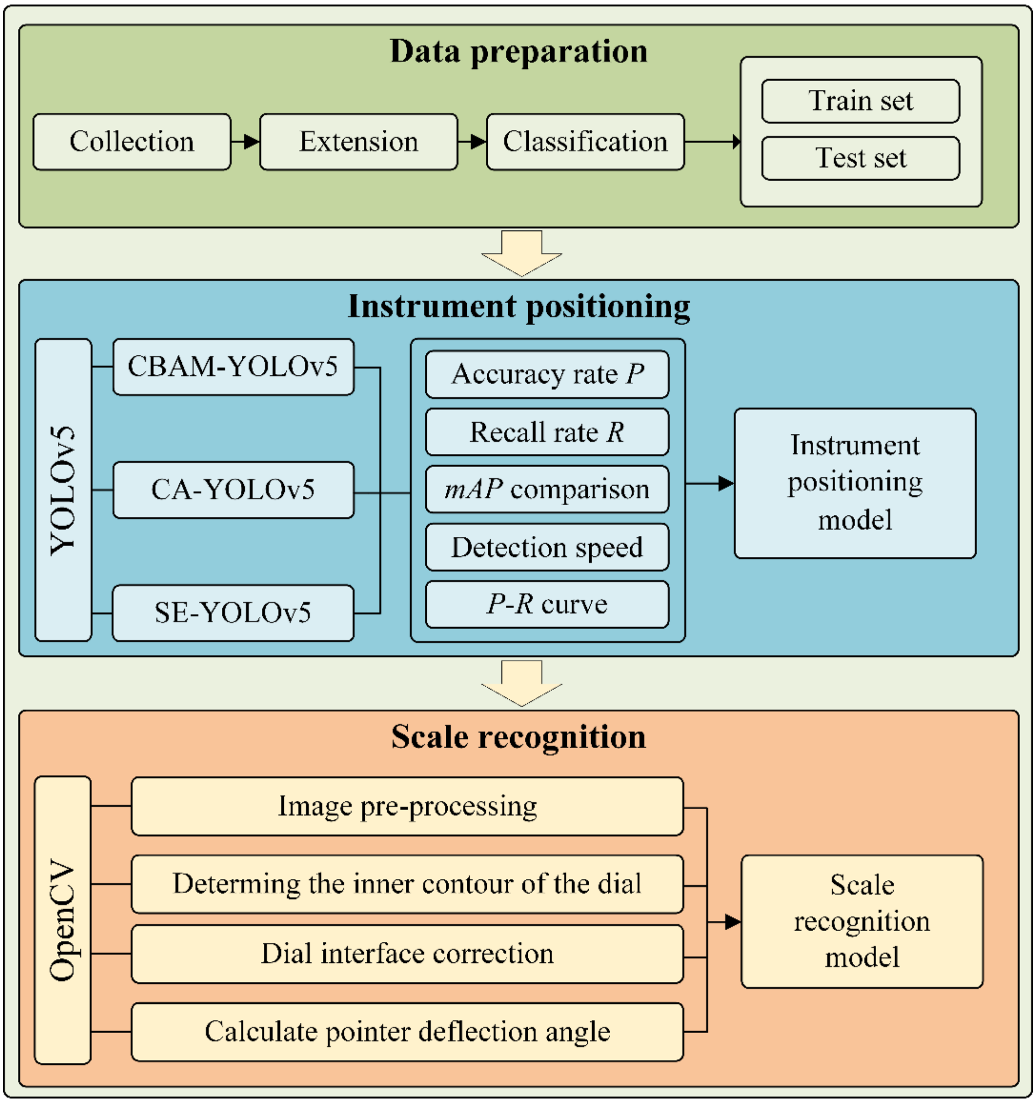

Figure 1. The Schematic Diagram of the Research Methodology for This Study.

2. Methods

This method incorporates an attention mechanism into the YOLOv5 detection model to significantly enhance the network's feature extraction capabilities and robustly localize the instrument area. During the scale recognition phase, we first apply perspective transformation correction to the tilted dial images, followed by scale reading, effectively enhancing the precision of instrument scale recognition.

2.1. Image Detection Model Based on Deep Learning

The YOLO series models, grounded in deep learning, are capable of performing object detection tasks. This paper introduces three prevalent attention mechanisms (Convolutional Block Attention Module (CABM), Coordinate Attention (CA), and Squeeze-and-Excitation (SE)) into the original YOLOv5 model. These mechanisms are, respectively, embedded into the layer preceding the SPPF (Spatial Pyramid Pooling-Fast) layer within the Backbone module. Consequently, three instrument localization models are derived: CABM-YOLOv5, CA-YOLOv5, and SE-YOLOv5, the structures of which are illustrated in Figure 2. In Figure 2, the CBS (ConvBNSiLU) module is responsible for extracting image features and is one of the fundamental modules used to build the backbone network of YOLOv5.

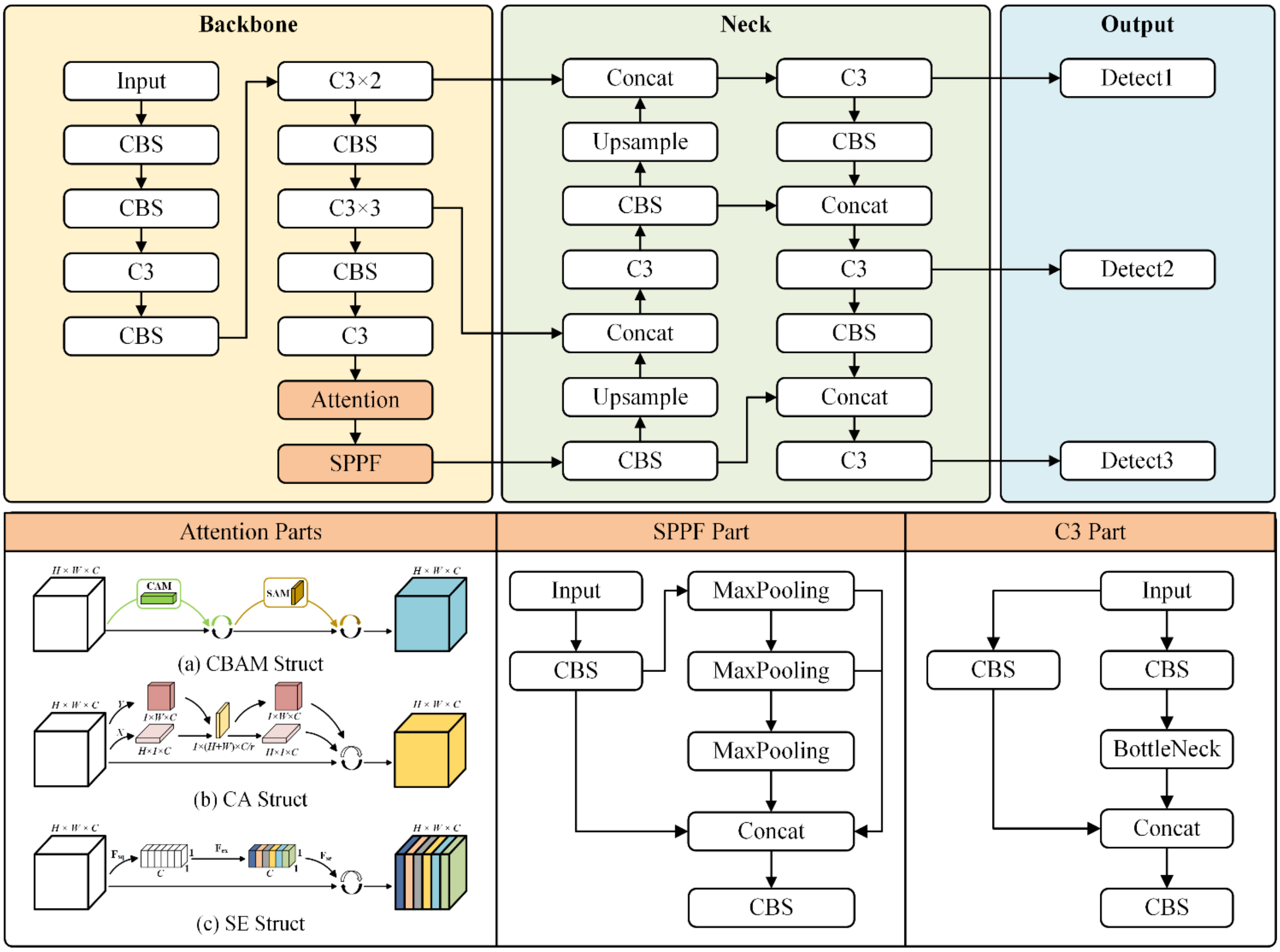

Figure 2. Illustration of Three Instrument Localization Models (CABM-YOLOv5, CA-YOLOv5, and SE-YOLOv5).

As Figure 2 indicates, upon receiving image data, the Backbone module employs attention mechanisms to further mine effective instrument features from the instrument feature map extracted by the original model in different ways:

(1) The CABM module computes attention maps for channel and spatial dimensions of the input feature map consecutively, and fuses them with the input feature map in sequence, achieving the goal of highlighting instrument features [21].

(2) The CA module conducts average pooling on the incoming feature map across the width and height dimensions, proceeds with a fusion process, then enlarges the results to secure attention weights for both axes, subsequently applying these weights to the input feature map to bolster the efficiency of extracting instrumental features [22].

(3) The SE module compresses, then excites, the input feature map followed by a calibration operation, making the model more sensitive to instrument features [23,24].

The image features extracted by the Backbone, along with their corresponding semantic information, are uploaded to the Neck module. This module performs feature fusion between top-level and bottom-level features to further enhance the representational effectiveness of the instrument characteristics. Ultimately, this process yields multi-class object detection data information, referred to as Detect.

2.2. Instrument Scale Recognition Method

The study proposes a method for recognizing the markings on instruments. Initially, it establishes a self-positioning method for the instrument panel to determine the contours within the panel. Subsequently, a method to correct the tilt of the scale dial is developed, where the dial is rotated for adjustments, resulting in a corrected image of the instrument panel that lays the groundwork for further analysis or recognition of the panel markings. Finally, a scale recognition algorithm is introduced to obtain the results for instrument scale recognition. The method for recognizing instrument scales is illustrated in Figure 3.

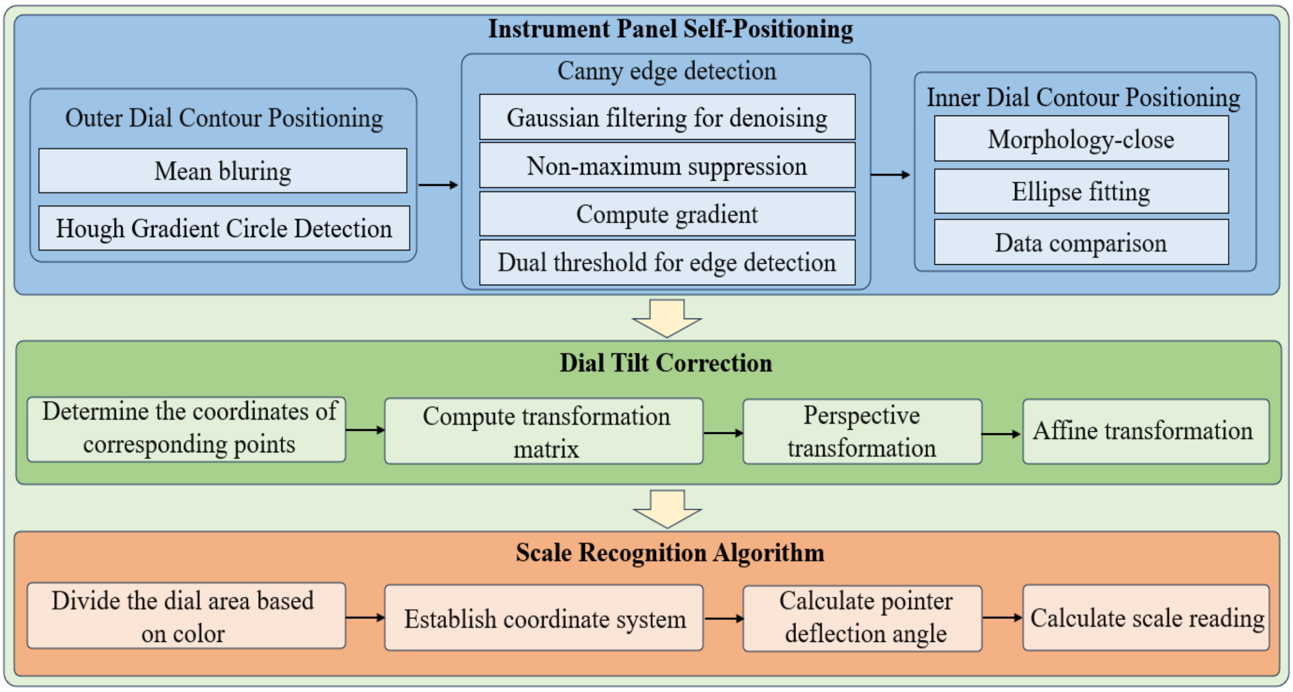

Figure 3. Instrument Scale Recognition Method Flowchart.

2.2.1. Instrument Panel Self-Positioning

After the identification and extraction of instruments using CA-YOLOv5, it is necessary to further extract the dial for improved scale recognition accuracy. Based on the structural characteristics of arrester pointer instruments, a method that first identifies the outer contour of the dial and then the inner contour is adopted for dial extraction. The process of inner dial contour extraction is illustrated in Figure 4.

(**a**) (**b**) (**c**)

Figure 4. The Process of Inner Dial Contour Extraction. (**a**) Gradient Circle Positioning; (**b**) Contour Extraction; (**c**) I nner Dial Contour Positioning. (Note: The Chinese characters in the image are as follows: Alarm, Model: JCQ-2/800, Surge Arrester Operation Detector, Date: March 2023, Number: 3831, Shanghai Leichuan Surge Arrester Co., Ltd.).

Step one involves performing mean blur on the input image to reduce the impact of random noise and quickly obtain the contour lines and the utilization of the Hough Gradient Circle Detection algorithm, as shown in Figure 4a to determine the location of the dial's outer contour. This step aims to reduce background interference and save data on the circle's center coordinates and radius.

In the second step, as illustrated in Figure 4b, Canny edge detection is applied to the image to filter the extracted contours, removing those that are small and irregular in area. The algorithm includes the following four steps: (1) Apply Gaussian filtering to remove noise from the image. (2) Compute the gradient magnitude and direction of the pixels in the image. (3) With the gradient magnitude and direction of the points known, perform non-maximum suppression to remove all non-edge points. (4) Set upper and lower thresholds to filter processed edges to determine the contour edges.

The third step conducts an elliptical fitting to the contours that have been filtered. Based on the data retained from step one, a further selection is performed on the fitted ellipse to finalize the inner contour of the dial, as depicted in Figure 4c. The data on the major and minor axes of the ellipse are saved to serve as a basis for calculating the perspective transformation of the dial in subsequent steps.

2.2.2. Dial Tilt Correction

If a disparity exists between the long and short axes of the inner dial contour, it indicates that the dial is tilted to varying degrees. To ensure the accuracy of subsequent scale recognition, it is necessary to perform a perspective transformation on the tilted dial to correct its alignment. Perspective transformation involves using matrix multiplication to project the original two-dimensional image into three-dimensional space and then map it onto a new two-dimensional plane. The perspective transformation process is depicted in Figure 5.

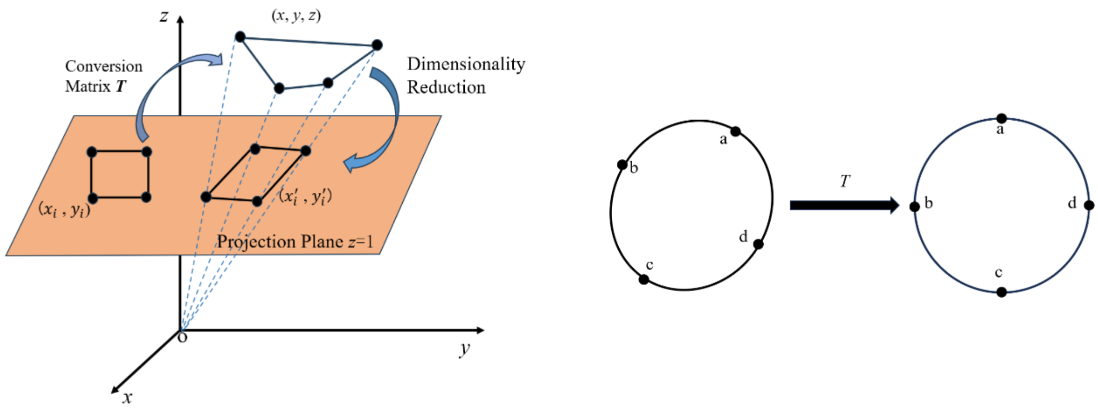

(**a**) (**b**)

Figure 5. Perspective Transformation. (**a**) Principle of perspective transformation; (**b**) Four sets of corresponding coordinate points.

The specific method is as follows: extend the original image coordinates with a z-coordinate to perform perspective transformation in three-dimensional space, and assume ($z_i' = z_i = 1$), which means that the spatial operation before and after remains on the plane (z = 1). The working principle is shown in Figure 5a, and the perspective transformation formula is as

$$\begin{bmatrix} x_i' \\ y_i' \\ 1 \end{bmatrix} = T \begin{bmatrix} x_i \\ y_i \\ 1 \end{bmatrix} = \begin{bmatrix} t_{11} & t_{12} & t_{13} \\ t_{21} & t_{22} & t_{23} \\ t_{31} & t_{32} & t_{33} \end{bmatrix} \begin{bmatrix} x_i \\ y_i \\ 1 \end{bmatrix} \tag{1}$$

i.e.,

$$\begin{aligned} x_i' &= \frac{t_{11}x_i + t_{12}y_i + t_{13}}{t_{31}x_i + t_{32}y_i + t_{33}} \\ y_i' &= \frac{t_{21}x_i + t_{22}y_i + t_{23}}{t_{31}x_i + t_{32}y_i + t_{33}} \end{aligned} \tag{2}$$

assume $t_{33} = 1$,

$$\begin{array}{c} t_{11}x_i + t_{12}y_i + t_{13} - t_{31}x_ix_i' - t_{32}y_ix_i' = x_i' \\ t_{21}x_i + t_{22}y_i + t_{23} - t_{31}x_iy_i' - t_{32}y_iy_i' = y_i' \end{array} \quad (3)$$

Obtains the coordinate information of the endpoints of the major and minor axes retained from the ellipse fitting process, as well as the coordinate information for the corresponding points on the major and minor axes after the perspective transformation into a circle, as shown in Figure 5b. By substituting these into equation (3), the transformation matrix T yielding:

$$T = \begin{bmatrix} t_{11} & t_{12} & t_{13} \\ t_{21} & t_{22} & t_{23} \\ t_{31} & t_{32} & t_{33} \end{bmatrix} = \begin{bmatrix} T_1 & T_2 \\ T_3 & t_{33} \end{bmatrix} \quad (4)$$

where T_1 denotes the image linear transformation, T_2 is used for generating the image perspective transformation, and T_3 represents the image translation. By substituting the computed transformation matrix T into equation (2), the resulting data of the dial coordinates after perspective transformation are obtained, yielding a corrected circular dial as shown in Figure 6, thereby achieving the rectification of the inclined instrument dial. Perspective transformation may lead to significant offset of the dial position in the corrected image and the scale not being centered. The counting rectangular frame in the dial can be detected and extracted, and an affine transformation can be applied to it to deduce the rotation angle. Subsequently, the dial is corrected for rotation based on the calculated rotation angle for subsequent image analysis or processing.

Figure 6. Perspective-transformed Image of the Instrument Panel. (Note: The Chinese characters in the image are as follows: Alarm, Model: JCQ-2/800, Surge Arrester Operation Detector, Date: March 2023, Number: 3831, Shanghai Leichuan Surge Arrester Co., Ltd.).

2.2.3. Scale Recognition Algorithm

After correcting the dial, the designated colors on the instrument scale are extracted and located, preserving the three colors of yellow, green, and red in the scale dial and eliminating the rest. The result is shown in Figure 7. By iterating over the scale bars, the coordinate data for all scale points are obtained and stored separately in array form, facilitating subsequent calculations of the instrument scale.

The process of recognizing the scale of a pointer-type surge arrester instrument is shown in Figure 8. The dial can be divided into regions I, II, III, and IV based on different scale colors. The distribution of scales between regions is uneven, but within each region, the scales are evenly distributed. When the pointer is in region II, a coordinate system is established as shown in Figure 8a. The result of scale recognition calculation based on the angular method is as follows.

$$V = A_i + \alpha_i \cdot \frac{M_i}{\beta_i} \quad (5)$$

Figure 7. Color Extraction of Scale Bars.

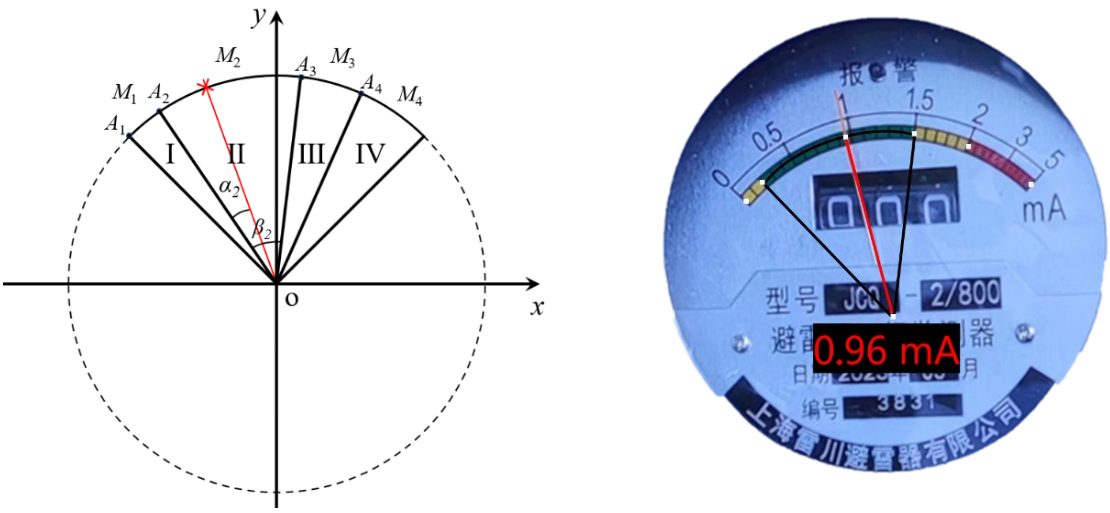

(**a**) (**b**)

Figure 8. The Process of Recognizing the Scale of a Pointer-type Surge Arrester Instrument. (**a**) The coordinate system; (**b**) Scale recognition results. (Note: The Chinese characters in the image are as follows: Alarm, Model: JCQ-2/800, Surge Arrester Operation Detector, Date: March 2023, Number: 3831, Shanghai Leichuan Surge Arrester Co., Ltd.)

A_i (wh 3, 4) are the starting scales for each region; α_i represents the deflection angle of the pointer from the starting line within its region; M_i is the scale range for an individual region; β_{i} is the angle corresponding to the scale range of an individual region. The scale recognition result is shown in Figure 8b.

2.3. Experimental Setup and Analysis

A total of 1000 images of surge arrester pointer-type instruments were captured in the field (resolution 600 × 800), and then randomly divided into 800 images for the training set and 200 images for the validation set. These images cover meter readings from different angles, backgrounds, and lighting conditions to ensure that the trained model has strong generalization ability. These were then fed into localization models with different attention mechanisms for training and detection. In this study, Table 1 enumerates the configuration parameters for both software and hardware utilized in the experiment.

This study utilizes evaluation metrics such as Precision (P), Recall (R), Average Precision (AP), and mean Average Precision (mAP) to evaluate the model's performance. The formulas for calculating these parameters are as follows.

Table 1. Configuration Parameters for Both Software and Hardware.

Name	Parameters
Operating System	Windows 10
CPU	AMD Ryzen7 5800H
GPU	NVIDIA GeForce RTX3070 8G
RAM	16 GB (8GB × 2)
Python	3.7.0
Pytorch	1.13.1
CUDA	11.3

Precision (P) is defined as the proportion of positive samples that the model correctly identifies out of the total positive samples that it identifies. The formula for calculation is

$$P = \frac{TP}{(TP + FP)} \tag{6}$$

where, TP represents the number of True Positives, and FP represents the number of False Positives.

Recall (R) is the measure of the model's correctly identified positive samples in relation to the total number of actual positive samples. The formula for calculation is

$$R = \frac{TP}{TP + FN} \tag{7}$$

where FN is the number of false negatives, which are the correct samples that were missed.

Average Precision (AP) denotes the mean of precision scores at various recall thresholds, typically derived by constructing a precision-recall curve and computing the area beneath this curve.

$$AP = \int_0^1 P(R)dR \tag{8}$$

where $P(R)$ is the P-R curve on the range [0,1].

Mean Average Precision (mAP) refers to the average of AP across all classes or queries, which is a common metric in the context of multiple classes or multiple queries. In some cases, mAP might also be the average of AP across all levels of detection difficulty or at different recall cut-off points:

$$mAP = \frac{\sum_{i=1}^{n} AP}{n} \tag{9}$$

where n is the number of categories.

These indicators offer an all-encompassing view for assessing the model's efficacy, taking into account the accuracy of the model's detections as well as its capacity to encompass positive samples.

3. Results

Under the same experimental conditions, the test set was input into three different meter positioning models—CBAM-YOLOv5, CA-YOLOv5, SE-YOLOv5—as well as the original YOLOv5 model for training and testing. The test results for each model are shown in Table 2.

Table 2. Test Results of Different Models.

Model.	Precision(P) /%	Recall (R) /%	mean Average Precision (mAP) /%	Test Time /ms
CBAM-YOLOv5	89.5	84.7	90.5	66.1
CA-YOLOv5	91.9	88.1	92.6	66.3
SE-YOLOv5	90.3	86.6	91.4	65.8
YOLOv5	88.8	76.4	88.6	65.3

The data presented in Table 2 reveal that the integration of the attention mechanism module, while adding to the complexity of the base model, has resulted in a longer average detection time for the CBAM-YOLOv5, CA-YOLOv5, and SE-YOLOv5 models relative to the standard YOLOv5 model. However, in terms of mean average precision (*mAP*), the CBAM-YOLOv5, CA-YOLOv5, and SE-YOLOv5 models have seen respective increases of 1.9%, 4%, and 2.8% compared to the original YOLOv5 model. This confirms that the inclusion of the attention mechanism module can enhance the capability of extracting key features, thereby improving recognition accuracy. The P-R curves of the four target detection models are shown in Figure 9.

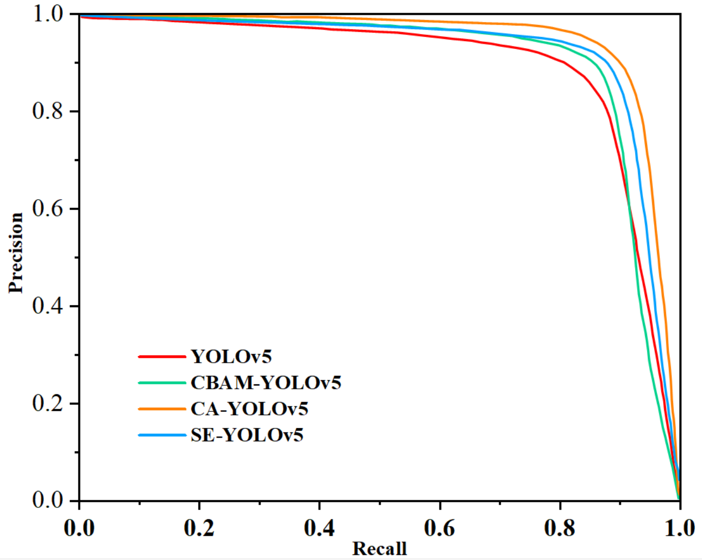

Figure 9. The *P-R* Curves of the Four Target Detection Models.

From Figure 9, it is evident that the *P-R* curve for the CA-YOLOv5 model covers the largest area, and its *AP* value, calculated using Equation (8), is 0.915. Based on the aforementioned four evaluation metrics, it can be seen that the CA-YOLOv5 model has stronger positioning capability in the task of instrument recognition compared to CBAM-YOLOv5, SE-YOLOv5, and YOLOv5. The positioning result of the CA-YOLOv5 target positioning model is shown in Figure 10.

Figure 10. The Positioning Result of the CA-YOLOv5 Target Positioning Model.

Combining the optimal object detection model CA-YOLOv5 with the scale recognition model, a complete meter scale recognition system can be obtained. Within this system, when an image is inputted, the object detection model CA-YOLOv5 is responsible for locating the meter and marking the location result with a red box. Subsequently, the marked section is inputted into the scale recognition model, which is in charge of extracting and correcting the dial, as well as calculating the deflection angle of the pointer, to ultimately obtain the scale reading results.

After model training is complete, it is necessary to perform scale recognition on the meter data in the test set, and to tally the success rate of meter scale recognition under different error thresholds e. The performance of different models is evaluated based on the average error w of the results and the time consumed. The expression for error threshold e and average error w are

$$e = \frac{|V - V'|}{h} \tag{10}$$

$$w = \frac{1}{200}\sum_{i=1}^{200} e_i \tag{11}$$

where V is the calculated result of the instrument scale; V' is the actual recognized result of the instrument scale; h is the unit scale of the area where the instrument needle is located. The recognition results of the test set are shown in Table 3.

Table 3. The Recognition Results of the Test Set.

Model	Error Threshold e				Average Error w/%	Consumed Time /s
	0.1	0.4	0.8	1.2		
CA-YOLOv5	7%	50%	81%	96%	0.923	0.662
SURF	5%	34%	68%	80%	1.612	0.933
U-net	5%	36%	71%	85%	1.276	1.024

In addition, binary descriptor-based SURF [25–27] and U-net technique [28,29] are being widely deployed for recognition systems. For comparison, the results identified by these two methods are also included in Table 3.

From Table 3, it can be seen that within the allowable range of error threshold, the success rate of arrester pointer instrument scale recognition by CA-YOLOv5 has greatly improved compared to the SURF recognition algorithm and the U-net model. With an error threshold of 1.2 times, the recognition success rate is as high as 96%, and the average error is 0.923%, indicating high accuracy and robustness. In terms of detection speed, the method takes an average of 0.662 s to detect instrument images, which is shorter than the other two scale recognition models. The test results show that the method proposed in this paper can recognize instrument scales against different backgrounds and distances, with not only a short processing time but also strong robustness and accuracy, meeting the practical application requirements for arrester pointer instrument scale recognition.

4. Discussion

The results of the research on the recognition method of dial scales for arrester pointer instruments present a significant advancement in the field of automated scale recognition using deep learning techniques. The integration of an attention mechanism into the YOLOv5 network architecture, coupled with OpenCV for image processing, has led to a high success rate of 96% in recognition with an average error rate of just 0.923%. These findings underscore the potential of deep learning to enhance the accuracy and efficiency of scale recognition tasks in complex environments.

The enhanced performance of the CA-YOLOv5 model in recognizing arrester pointer instruments is attributed to the improved feature extraction from the attention mechanism. This finding is consistent with other research showing the benefits of attention mechanisms in deep learning models. The attention mechanism allows the model to focus on more relevant features within the image, thus reducing the influence of background noise and increasing the robustness of the recognition process.

The success of the attention-enhanced YOLOv5 models over traditional methods like the SURF recognition algorithm and U-net model is particularly notable. While the SURF and U-net techniques are dependable and widely used, the proposed CA-YOLOv5 model outperforms them, not just in terms of recognition rate, but also in processing time. This suggests that the use of attention mechanisms in combination with convolutional neural networks is a promising direction for real-time image recognition tasks.

The implications of this study are twofold. Firstly, the application of the CA-YOLOv5 model can significantly reduce the time and resources spent on manual scale readings, minimizing human error and optimizing the operational efficiency of substation facilities. Secondly, the methodology can be generalized to other types of instruments and scenarios that require rapid and accurate scale detection, thus broadening the scope of automated industrial monitoring systems.

The practical application of these findings could include integration into real-time monitoring systems for substations, contributing to improved predictive maintenance and reliability of electrical power networks. Furthermore, the methodology could be adapted to other fields such as medical imaging, where precision and speed are critical.

Further research could explore the integration of more sophisticated attention mechanisms or the combination of different deep learning models to improve recognition rates even further. It also presents the opportunity to study the model's performance in larger, more diverse datasets to ensure its robustness and scalability.

5. Conclusions

In this study, we have innovatively incorporated a CA (Channel Attention) attention mechanism module into the YOLOv5 object detection model framework. This module significantly enhances the model's proficiency in extracting relevant features, which is particularly crucial for the accurate recognition and localization of arrester pointer-type instruments. Leveraging the OpenCV library, we carried out meticulous dial correction, which significantly refined the accuracy of scale recognition.

Despite the introduction of the attention mechanism module contributing to an increase in the model's complexity—and consequently, a slight uptick in the average detection time for the modified CBAM-YOLOv5, CA-YOLOv5, and SE-YOLOv5 models in comparison to the baseline YOLOv5 model—the trade-off has proven to be beneficial. The improvements in mean average precision (*mAP*) are noteworthy, with increases of 1.4%, 4%, and 2.8% for the aforementioned models, respectively. These metrics not only validate the efficacy of the attention mechanism in bolstering the extraction of essential features but also showcase the potential for more sophisticated object detection capabilities in complex real-world scenarios.

Our rigorous testing on a specialized dataset of arrester pointer-type instruments yielded impressive results. The proposed method for scale recognition attained a remarkably high success rate of 96% within the defined acceptable error margin. Moreover, the method maintained an impressively low average error rate of 0.923% while operating at commendable speeds, averaging a mere 0.662 s for image processing. This performance surpasses that of conventional methods, such as the SURF (Speeded Up Robust Features) recognition algorithm and the U-net model, by a significant margin. The notable improvements in accuracy and speed clearly demonstrate the superiority of our method, confirming its potential for widespread adoption in practical applications where rapid and precise scale recognition is paramount.

In conclusion, the study successfully addresses the challenges posed by the recognition of arrester pointer instruments in various scenarios. The CA-YOLOv5 model's impressive accuracy and efficiency in recognizing dial scales against diverse backgrounds and distances demonstrate the power of deep learning in complex pattern recognition tasks. The thorough validation of the proposed method against a specialized dataset confirms its viability for practical application and sets a new benchmark for automated scale recognition technology.

This study represents a substantial contribution to the automation of substation monitoring and opens up new avenues for research and development in intelligent industrial systems.

Author Contributions: Conceptualization, H.W. and H.Y.; methodology, H.Y.; software, Y.H.; investigation, Y.H.; resources, H.W.; data curation, Y.H.; writing—original draft preparation, H.W.; writing—review and editing, Y.C.; visualization, Y.C.; supervision, H.W.; project administration, H.W.; funding acquisition, H.W. All authors have read and agreed to the published version of the manuscript.

Funding: This research was funded by the National Science Foundation of China (grant number 12172255), Tianjin Science and Technology Plan Project (grant number 23YDTPJC00390) and Tianjin Municipal Education Commission Scientific Research Plan Project (grant number 2022ZD002).

Institutional Review Board Statement: Not applicable.

Informed Consent Statement: Not applicable.

Data Availability Statement: The raw data supporting the conclusions of this article will be made available by the authors on request.

Conflicts of Interest: The authors declare no conflicts of interest.

Abbreviations

Abbreviations and full names utilized thought the manuscript.

Abbreviation	**Full name**
YOLOv5	You Only Look Once version 5
OpenCV	Open Source Computer Vision Library
SPPF	Spatial Pyramid Pooling-Fast
CBAM	Convolutional Block Attention Module
CA	Channel Attention
SE	Squeeze-and-Excitation
R-CNN	Region-based Convolutional Neural Network
WSN	Wireless Sensor Network
YOLOX-CAlite	A variation of the YOLOX model with a particular lite attention mechanism
Yolov7	You Only Look Once version 7
YLU2-Net	A combination of YOLOv5 and the U-2-Net network
Faster R-CNN	Faster Region-based Convolutional Network
SURF	Speeded Up Robust Feature
U-net	A type of convolutional neural network designed for biomedical image segmentation
Lite-FCOS	A lightweight variant of FCOS (Fully Convolutional One-Stage Object Detection)
CNN	Convolutional Neural Network
AP	Average Precision
mAP	Mean Average Precision
YOLO	You Only Look Once: A real-time object detection system that views object detection as a single regression problem
SAM	Spatial Attention Module
CAM	Channel Attention Module
CBS	ConvBNSiLU

References

1. Huo, F.C.; Li, A.; Ren, W.J.; Wang, D.; Yu, T. New identification method of linear pointer instrument. *Multimed. Tools Appl.* **2023**, *82*, 4319–4342. [CrossRef]
2. Li, Z.H.; Yu, Y.; Jin, B.H.; Cui, Y.H. Automatic reading recognition of pointer barometer based on machine vision. *J. Electronic Imaging* **2022**, *31*, 051415. [CrossRef]
3. Wang, Q. Automatic pointer meters recognition system based on line scan vision. *Meas. Sci. Technol.* **2022**, *33*, 127001. [CrossRef]
4. Ma, Y.F.; Jiang, Q. A robust and high-precision automatic reading algorithm of pointer meters based on machine vision. *Meas. Sci. Technol.* **2019**, *30*, 015401. [CrossRef]

5. Peng, G.; Du, B.; Cao, C.; He, D.X. Pointer-type instrument positioning method of intelligent inspection system for substation. *J. Electron. Imaging* **2022**, *31*, 013001. [CrossRef]
6. Li, D.H.; Li, W.X.; Yu, X.; Gao, Q.; Song, Y. Automatic reading algorithm of substation dial gauges based on coordinate positioning. *Appl. Sci.* **2021**, *11*, 6059. [CrossRef]
7. Guo, X.M.; Zhu, Y.P.; Zhang, J.; Hai, Y.; Ma, X.F.; Lv, C.Y.; Liu, S.P. Intelligent pointer meter interconnection solution for data collection in farmlands. *Comput. Electron. Agr.* **2021**, *182*, 105985. [CrossRef]
8. Yang, C.J.; Zhu, R.J.; Yu, X.D.; Yang, C.; Xiao, L.J.; Fowler, S. Real-time reading system for pointer meter based on YolactEdge. *Connect. Sci.* **2023**, *35*, 2241669. [CrossRef]
9. Wu, S.K.; Zhang, S.H.; Jing, X.D. An industrial meter detection method based on lightweight YOLOX-CAlite. *IEEE Access* **2023**, *11*, 3573–3583. [CrossRef]
10. Zhang, C.L.; Shi, L.; Zhang, D.D.; Ke, T.; Li, J.R. Pointer meter recognition method based on Yolov7 and hough transform. *Appl. Sci.* **2023**, *13*, 8722. [CrossRef]
11. Liu, H.L.; Wang, J.L.; Ma, B. Instrument pointer recognition scheme based on improved CSL algorithm. *Sensors* **2022**, *22*, 7800. [CrossRef]
12. Chen, L.S.; Wu, X.; Sun, C.; Zou, T.; Meng, K.; Lou, P.H. An intelligent vision recognition method based on deep learning for pointer meters. *Meas. Sci. Technol.* **2023**, *34*, 055410. [CrossRef]
13. Zhang, H.F.; Chen, Q.Q.; Lei, L.T. A YOLOv3-based industrial instrument classification and reading recognition method. *Mob. Inf. Syst.* **2022**, *2022*, 7817309. [CrossRef]
14. Liu, Y.; Liu, J.; Ke, Y.C. A detection and recognition system of pointer meters in substations based on computer vision. *Measurement* **2020**, *152*, 107333. [CrossRef]
15. Cai, W.D.; Ma, B.; Zhang, L.; Han, Y.M. A pointer meter recognition method based on virtual sample generation technology. *Measurement* **2020**, *163*, 107962. [CrossRef]
16. Zuo, L.; He, P.L.; Zhang, C.H.; Zhang, Z.H. A robust approach to reading recognition of pointer meters based on improved mask-RCNN. *Neurocomputing* **2020**, *388*, 90–101. [CrossRef]
17. Hou, L.Q.; Qu, H.S. Automatic recognition system of pointer meters based on lightweight CNN and WSNs with on-sensor image processing. *Measurement* **2021**, *183*, 109819. [CrossRef]
18. Wang, L.; Wang, P.; Wu, L.H.; Xu, L.J.; Huang, P.; Kang, Z.L. Computer vision based automatic recognition of pointer instruments: Data set optimization and reading. *Entropy* **2021**, *23*, 272. [CrossRef] [PubMed]
19. Zhou, D.K.; Yang, Y.; Zhu, J.; Wang, K. Intelligent reading recognition method of a pointer meter based on deep learning in a real environment. *Meas. Sci. Technol.* **2022**, *33*, 055021. [CrossRef]
20. Wang, Z.L.; Tian, L.F.; Du, Q.L.; An, Y.; Sun, Z.Z.; Liao, W.Z. Scale value guided Lite-FCOS for pointer meter reading recognition. *Meas. Sci. Technol.* **2023**, *34*, 125405. [CrossRef]
21. Agac, S.; Incel, O.D. On the use of a convolutional block attention module in deep learning-based human activity recognition with motion sensors. *Diagnostics* **2023**, *13*, 1861. [CrossRef]
22. Xie, F.; Lin, B.J.; Liu, Y.C. Research on the coordinate attention mechanism fuse in a YOLOv5 deep learning detector for the SAR ship detection task. *Sensors* **2022**, *22*, 3370. [CrossRef]
23. Rajendran, T.; Valsalan, P.; Amutharaj, J.; Jenifer, M.; Rinesh, S.; Latha, G.C.P.; Anitha, T. Hyperspectral image classification model using squeeze and excitation network with deep learning. *Comput. Intel. Neurosc.* **2022**, *2022*, 9430779. [CrossRef]
24. Hu, J.; Shen, L.; Albanie, S.; Sun, G.; Wu, E.H. Squeeze-and-excitation networks. *IEEE Trans. Pattern Anal. Mach. Intell.* **2020**, *42*, 2011–2023. [CrossRef] [PubMed]
25. Vinay, A.; Vasuki, V.; Bhat, S.; Jayanth, K.S.; Murthy, K.N.; Natarajan, S. Two dimensionality reduction techniques for SURF based face recognition. *Procedia Comput. Sci.* **2016**, *85*, 241–248. [CrossRef]
26. Li, X.G.; Zhu, J.; Ruan, Y.M. Vehicle seat detection based on improved RANSAC-SURF algorithm. *Int. J. Pattern Recogn.* **2021**, *35*, 2155004. [CrossRef]
27. Bay, H.; Ess, A.; Tuytelaars, T.; Van Gool, L. Speeded-up robust features (SURF). *Comput. Vis. Image Underst.* **2008**, *110*, 346–359. [CrossRef]
28. Zunair, H.; Ben Hamza, A. Sharp U-Net: Depthwise convolutional network for biomedical image segmentation. *Comput. Biol. Med.* **2021**, *136*, 104699. [CrossRef] [PubMed]
29. Shao, J.Q.; Chen, S.W.; Zhou, J.; Zhu, H.S.; Wang, Z.Y.; Brown, M. Application of U-Net and optimized clustering in medical image segmentation: A review. *CMES Comp. Model. Eng.* **2023**, *136*, 2173–2219. [CrossRef]